

Evaluation of VSPAERO Analysis Capabilities for Conceptual Design of Aircraft with Propeller-Blown Wings

Carla N. D. Sheridan¹, Dahlia D. V. Pham²

Universities Space Research Association, Hampton, Virginia, 23666, United States

Siena K. S. Whiteside³

NASA Langley Research Center, Hampton, Virginia, 23666, United States

Advancements in electric propulsion and the emergence of Advanced Air Mobility are driving the evolution of new aircraft designs. Since electric propulsion enables flexibility in propeller location, there is an increasing need for reliable, quick analyses of propeller-airframe interactions during the conceptual design phase. Many existing analysis tools capable of accurately modeling propeller-airframe interactions are computationally expensive and require a high level of expertise and significant time investment for setup. VSPAERO is a NASA-developed, open source, computational analysis tool that runs a Vortex-Lattice Method (VLM) solver and is targeted at conceptual design. This paper assesses the applicability of the VSPAERO VLM in the conceptual design phase by comparing VSPAERO predictions to predictions by OVERFLOW, a Reynolds-Averaged Navier-Stokes Computational Fluid Dynamics solver, and RoBIN, another VLM tool. The paper details the modeling, meshing, and analysis techniques used within VSPAERO. Analyses were performed for a wing in isolation, a propeller in isolation, and then for two propeller-blown wing configurations: one with a propeller located at the midspan and another with a propeller located at the wingtip. The propeller was modeled both as an actuator disk and as rotating blades.

I. Nomenclature

α	=	angle of attack
ρ	=	air density
C_P	=	coefficient of power, $C_P = \frac{P}{\rho N^3 D^5}$
C_p	=	pressure coefficient
C_T	=	coefficient of thrust, $C_T = \frac{T}{\rho N^2 D^4}$
D	=	propeller diameter
D_i	=	induced drag
L	=	lift
M	=	moment
N	=	number of revolutions per second
n	=	integer multiple for W-direction tessellation
P	=	power
T	=	thrust
$(x, y, z)_{comp}$	=	x, y, or z component location in the aft, right, up convention

¹ NIFS Intern, Aeronautics Systems Analysis Branch, 1 N. Dryden St. MS 442, AIAA Member.

² NIFS Intern, Aeronautics Systems Analysis Branch, 1 N. Dryden St. MS 442, AIAA Member.

³ Aerospace Engineer, Aeronautics Systems Analysis Branch, 1 N. Dryden St. MS 442, AIAA Member.

II. Introduction

Electric propulsion has opened the design space for countless new aircraft configurations and technologies, as well as enabling concepts of operation such as Advanced Air Mobility (AAM) [1]. Because electric propulsion enables flexibility in propeller location, there is an increasing need for propeller-airframe interactions to be reliably and rapidly analyzed during the early design phases. Many existing analysis tools capable of accurately modeling propeller-airframe interactions are computationally expensive and require a high level of expertise and significant time investment for setup.

The purpose of this paper is to investigate the capabilities of VSPAERO [2], a vorticity-based flow solver, in modeling two specific propeller-blown wing configurations as a first step to assess its viability for conceptual aircraft design applications. The study may help designers to understand whether VSPAERO may be of use to them, since there are currently few publicly available validation cases for VSPAERO. The two configurations investigated are represented in Fig. 1. The configurations both consist of a finite wing with a single propeller in front of the wing: Configuration 1 has the propeller located at the midspan of the wing and the propeller shaft axis slightly below the wing chord; Configuration 2 has the propeller located at the wingtip and the propeller shaft axis coincident with the wing chord. The wing and propeller in isolation were also analyzed.

Analyses performed for this paper implemented the Vortex Lattice Method (VLM) in VSPAERO [2] and the propeller was modeled both as an actuator disk and as rotating blades. The predictions were compared with existing predictions by RoBIN [3], another NASA VLM code; and OVERFLOW [4], a Navier-Stokes Computational Fluid Dynamics (CFD) Solver developed by NASA. The corresponding RoBIN and OVERFLOW predictions can be found in Ref. [5]. The geometry for each configuration was created with OpenVSP [6]. Only lifting surfaces were included in the geometry, because VLM solvers do not generally attach trailing wakes to bluff bodies and therefore do not contribute to lift and induced drag.

This paper describes the tools investigated, the analysis setup for the VSPAERO predictions, and the mesh convergence studies completed to determine suitable mesh settings. The resulting VSPAERO predictions are then compared with OVERFLOW and RoBIN predictions and an account of the computational times required for each method is given.

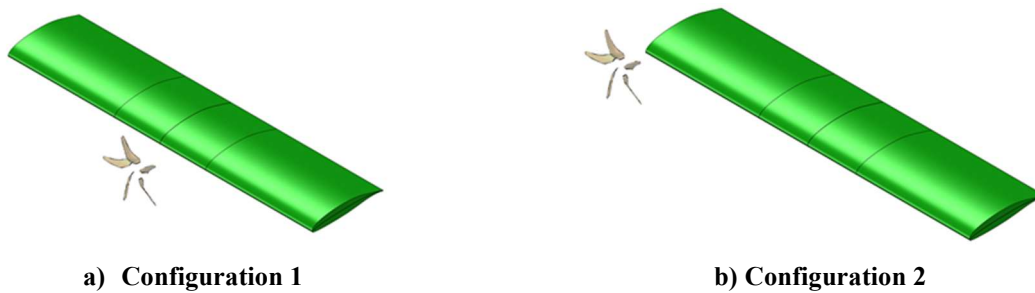


Fig. 1 Propeller-blown wing geometries.

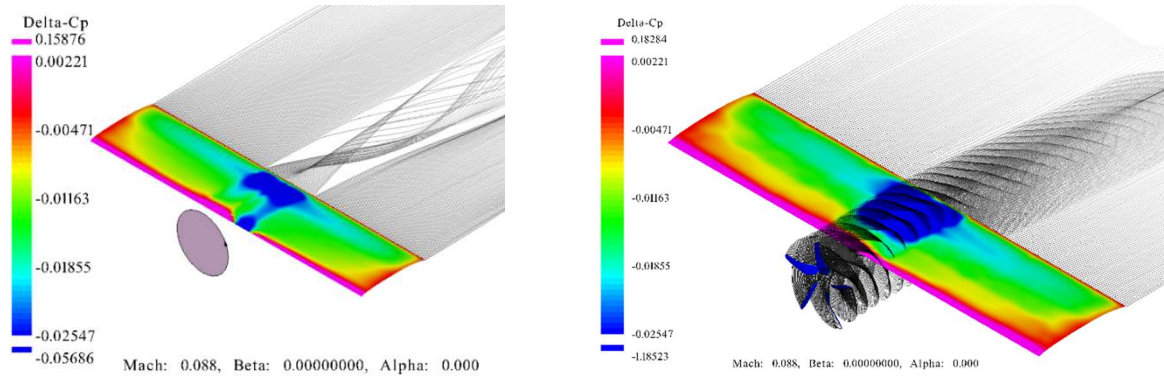
III. Tool Description

This section describes the three aerodynamic analysis tools compared in this paper. The predictions that were used as a baseline for comparison in this paper came from CFD that uses the full Navier-Stokes equations to solve aerodynamic loads on a geometry, conserving mass, momentum and energy. This is a high-fidelity method but is computationally expensive. VLMs use a camber surface representation to solve linear, inviscid, and irrotational flows, only conserving mass, but generate solutions much faster. It is recognized that CFD does not provide a replacement for wind tunnel testing; however, since this study is assessing tools to use in the conceptual design phase it is expected that CFD predictions provide a sufficiently realistic baseline for comparison.

A. VSPAERO

VSPAERO [2] is an open source tool developed by NASA [7] that is integrated with OpenVSP [6], a parametric aircraft geometry design and analysis tool. OpenVSP version 3.22.0 was utilized for this study. VSPAERO analyses can be performed on OpenVSP model geometries using a VLM or a panel method, and propellers can be modeled as actuator disks or rotating blades. VSPAERO predictions were performed with the VLM only; the panel method cannot model a wing and an actuator disk, or wing and rotating propeller blades. Actuator disks are implemented in VSPAERO as a differential pressure across the disk with constant axial velocity following conservation of momentum

[8], with an additional contribution of turning flow in the slipstream (“swirl”) as described by the Conway model [9]. Rotating blades are modeled as VLM surfaces with attached wakes that rotate over time. The wakes from the rotating blades can also interact with other bodies in the flow. Although VLM is a fundamentally inviscid method, VSPAERO also contains viscous corrections for lifting surfaces that are derived from an empirical fit of NACA 0012 airfoil data, but only inviscid results were evaluated in this study because the current version of VSPAERO does not differentiate viscous corrections from the total parasite drag estimate, and VSPAERO’s automatic parasite drag estimates are not directly applicable to propeller-blown wings [10]. A visualization of the VSPAERO VLM solver with the propeller represented as an actuator disk and as rotating blades is shown in Fig. 2, where the contours represent the difference in pressure coefficient (“delta-Cp”) across the vortex lattice.



a) Midspan propeller modeled as an actuator disk b) Midspan propeller modeled as rotating blades

Fig. 2 VSPAERO results visualizations of Configuration 1 with a VLM wing.

B. RoBIN

RoBIN is a VLM tool developed at NASA [5]. It is based on Katz and Plotkin’s vortex ring formulation [11]. RoBIN models propellers as rotating blades. Wakes are treated as freely deforming vortex sheets shed from the trailing edge. A visualization of Configuration 1 as modeled in RoBIN is shown in Fig. 3. The RoBIN setup is detailed in Ref. [5].

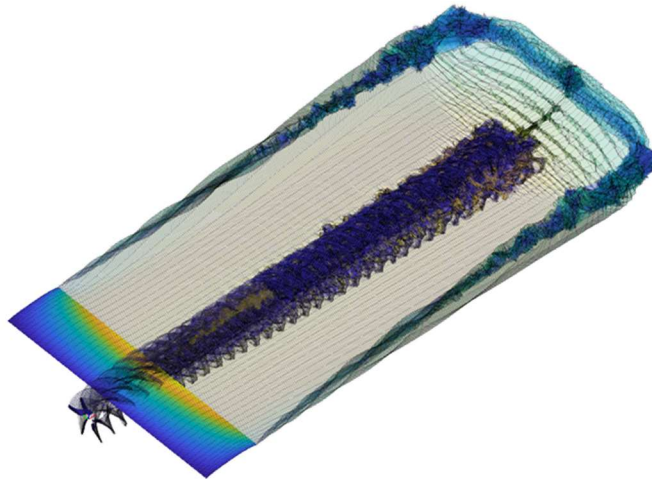


Fig. 3 RoBIN solver visualization of Configuration 1 with a VLM wing with VLM blades.

C. OVERFLOW

OVERFLOW, OVERset grid FLOW solver, is a high-fidelity CFD solver. Developed by NASA, it is a structured, overset grid system that uses Reynolds-Averaged Navier-Stokes solvers to perform aerodynamic analyses [4, 12]. Runs were performed by modeling the propeller geometry in OpenVSP, exporting it in a PLOT3D format for gridding, and using Chimera Grid Tools (CGT) [13] to assemble the overset grids for CFD analysis. Inviscid and viscous flux were calculated using a fifth order Weighted Essentially Non-Oscillatory method (WENO5M) [14] and second-order

central differences, respectively. The OVERFLOW setup is detailed in Ref. [5]. An example visualization of the OVERFLOW solution in Tecplot is provided in Fig. 4.

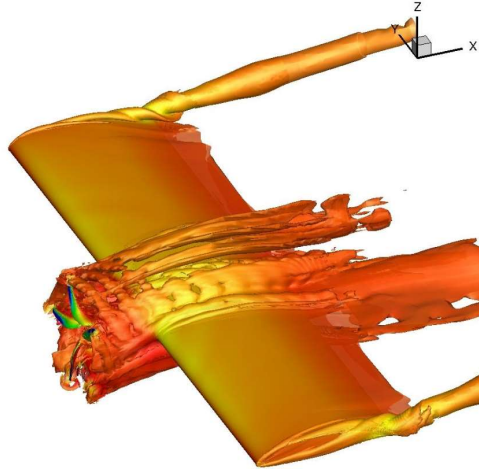


Fig. 4 OVERFLOW solver visualization of Configuration 1 with rotating blades.

IV. Methodology

This section outlines the geometry definitions, flow conditions, and setup techniques used for VSPAERO. The RoBIN and OVERFLOW methodology, setup, and predictions are detailed in Ref. [5].

A. Geometry Definitions and Flow Conditions

Geometry parameters for Configuration 1 and Configuration 2 are provided in Table 1. The global origin of the OpenVSP geometry is at the midspan of the wing leading edge, with the X axis in the chordwise direction towards the trailing edge, the Y axis in the spanwise direction towards the right wingtip, and the Z axis vertically upwards. The moment reference point for the wing is at the wing quarter-chord, and the moment reference point for the propeller is at the propeller center. The propeller axes of rotation are aligned with the global X, Y and Z axes. The rectangular wing employs the X-57 wing root airfoil [15]; the propeller is an X-57 High-Lift Propeller [16]. The OpenVSP geometry model may be accessed from the OpenVSP Hangar [17]. The flow conditions used in this study are presented in Table 2.

Table 1 Wing and Propeller Geometry

	Configuration 1	Configuration 2
Wing Chord (m)	0.7141	
Wing Span (m)	3.048	
Wing Area (m ²)	2.1767	
Wing Quarter Chord: X, Y, Z Location (m)	0.1786, 0.000, 0.000	
Number of Propeller Blades	5	
Propeller Diameter (m)	0.576	
Propeller Blade Root Diameter (m)	0.1168	
Propeller Center: X, Y, Z Location (m)	-0.259, 0.000, -0.108	-0.259, 1.524, 0.000

Table 2 Flow Conditions

Parameter (Units)	VSPERO GUI Input	Value
Angle of Attack (degrees)	“Alpha”	-5, 0, 5, 10, 15, 20
Mach Number	“Mach Start”	0.087674
Revolutions per Minute	“RPM”	4550
Reynolds Number	“ReCref”	622,610
Temperature, (K)	-	288.15
Altitude, (m)	-	0

B. VSPAERO Analysis Setup

VSPAERO analyses were performed by running “*.vpscript” files in OpenVSP. Several analysis settings were consistent across all VSPAERO runs; these are outlined in Table 3.

Table 3 Settings Used Across All VSPAERO Runs

Parameter	Definition	Input	Justification
Batch Calculation Flag	Sweeps through parameters in one run	On	Saves time, allows data to be processed more easily
X-Z Symmetry Flag	Runs simulation on half of the geometry and then mirrors	Off	Configurations tested were not symmetric
2 nd Order Karman-Tsien Mach Correction Flag	Compressibility correction factor (if toggled off, uses Prandtl Glauert correction)	On	Default setting, not relevant as flow conditions are subsonic
Num Iterations	Number of iterations	40	It was found that the default setting (5 iterations) was not sufficient for convergence
Wake Nodes	Number of nodes needed to capture curvature of trailing wakes	128	It was found that 128 wake nodes sufficiently captured trailing wake curvature
Far Field Distance	Distance of trailing wakes	50	Distance was set to capture 8 propeller revolutions in the trailing wakes (consistent with wake distance used for other tools in this study)

VSPAERO analyses solved for a steady-state solution for runs that did not include the propeller modeled as rotating blades. When the propeller was modeled as rotating blades, VSPAERO was run in unsteady mode, which is time dependent.

For all runs that included propellers modeled either as actuator disks or rotating blades, VSPAERO required additional inputs specific to the propeller, which are presented in Table 4. These propeller-specific inputs include freestream velocity, “Vinf,” freestream density, “Rho,” and an optional reference velocity, “VRef,” and reference Mach number, “MachRef.” When “VRef” is flagged on, “MachRef” is also flagged on. “Vinf” and “Rho” were set to the global freestream velocity and density, respectively, and “VRef” and “MachRef” were set to the propeller tip speed. VSPAERO uses the reference Mach number “MachRef” for compressibility corrections.

Table 4 Mach and Velocity Inputs

Parameter (Units)	VSPERO GUI Input	Value
Freestream Velocity (m/s)	“Vinf”	27.84
Air Density (kg/m ³)	“Rho”	1.225
Propeller tip speed (m/s)	“VRef”	137.16
Reference Mach Number	“MachRef”	0.403

For runs using an actuator disk, input values for C_T and C_P at each angle of attack were taken from the OVERFLOW predictions for the rotating propeller in Configuration 1 and Configuration 2; the corresponding C_T and C_P values are shown in Table 5.

Table 5 Coefficients of Thrust and Power

α (degrees)	Configuration 1		Configuration 2	
	C_T	C_P	C_T	C_P
-5	0.282	0.308	0.275	0.303
0	0.281	0.308	0.274	0.303
5	0.286	0.310	0.275	0.303
10	0.291	0.312	0.278	0.304
15	0.299	0.315	0.283	0.306
20	0.308	0.317	0.291	0.309

For runs with rotating propeller blades, the “Uniform RPM”, “Auto Time Step”, and “From Steady State” flags were set to “on”. Three propeller revolutions were used for the isolated propeller, and eight revolutions were used for the propeller-blown wing analyses. Eight revolutions were used for the propeller-blown wing analyses to capture interactions of the propeller wake with the wing. The “Auto Time Step” flag fixes the time steps to be equivalent to every 15 degrees of propeller rotation. If the “Auto Time Step” flag is off, manual inputs of time step and total number of time steps are required. Manual inputs were tested for the rotating blade predictions with time steps every 5 degrees of propeller rotation, but the results did not converge. When “Auto Time Step” was flagged on, the results converged.

Since runs with actuator disks were under steady conditions, whereas runs with propeller blades were under unsteady conditions, different output files and post-processing methods were used to extract the VSPAERO results. For the unsteady runs with the propeller modeled as rotating blades, VSPAERO outputs the full time history of the computed force and moment coefficients for the full configuration in the “*.history” files, and a component-level breakdown of those results in “*.group.*” files. The “*.group.*” files end in either “1” or “2” depending on whether the results are for the wing or propeller component, respectively. Moment coefficients in the “*.group.*” files are calculated based on the local reference location and axes for that component, as defined in the geometry in OpenVSP. When post-processing the data for the unsteady results, the force and moments coefficients were averaged over the last revolution of the propeller, represented by the last 24 time steps.

For the steady runs, the forces and moment coefficients at all angles of attack were parsed from the output “*.polar” file, which gives the results for the last iteration. However, it was found that the “*.polar” output file for the forces and moments did not account for actuator disk thrust. Therefore, in processing the data, the actuator disk thrust and torque components were derived from the input C_T and C_P values (Table 5), and then added to the wing forces and moments to obtain total forces and moments, as expressed in Eqs. 1-5. Note that since the actuator disk does not produce forces in its plane, in-plane forces are not included in these equations.

$$L_{total} = L_{wing} + T \sin(\alpha) \quad (1)$$

$$D_{i_{total}} = D_{i_{wing}} - T \cos(\alpha) \quad (2)$$

$$M_{x_{total}} = M_{x_{wing}} + M_{x_{prop}} \quad (3)$$

$$M_{y_{total}} = M_{y_{wing}} + T(z_{wing} - z_{prop}) \quad (4)$$

$$M_{z_{total}} = M_{z_{wing}} + T(y_{prop} - y_{wing}) \quad (5)$$

V. Mesh Convergence Studies

Mesh convergence studies were performed to investigate VSPAERO’s convergence behavior. Mesh convergence studies were important to ensure that the magnitudes of the output forces and moments were converged with respect to mesh settings; i.e., changes in the number of mesh panels would not change the results of the analysis. From the results of the mesh study, mesh parameters were selected that would achieve sufficiently converged results while minimizing simulation run times as much as possible. However, to minimize contributions from the mesh settings to inaccuracies in the predictions, higher panel counts were chosen than may be needed for other applications in which a designer may find lower panel counts to be acceptable in order to obtain results in less time.

Two mesh convergence studies were performed: for the wing in isolation and for the rotating blades in isolation. All of the mesh convergence studies were performed using the flow conditions specified in Table 2 and angles of attack of 0 and 10 degrees only; input parameters were the same as those outlined in Section IV Part B.

A. Meshing Parameters in OpenVSP

For wings and for propellers modeled as rotating blades, mesh parameters that can be adjusted in OpenVSP include (1) the mesh refinement in the chordwise and spanwise directions and (2) the clustering of panels towards the root, tip, leading edge, and/or trailing edge.

The input in OpenVSP for the number of nodes in the spanwise direction is denoted “Num_U,” and the input for the number of nodes in the chordwise direction is denoted “Num_W.” The number of panels in each direction are equal to the number of nodes minus one. In the chordwise direction, Num_W covers both the upper and lower surfaces so when using the VLM mode, the number of chordwise panels will be equal to $(Num_W - 1) / 2$. Num_W is constrained to the set of values defined by Eq. (6) for a wing and by Eq. (7) for a propeller blade, where n is an integer.

$$Num_W = 4n + 1, \tag{6}$$

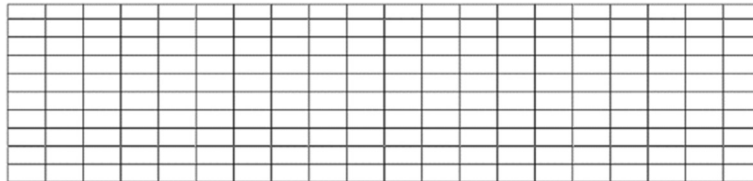
$$Num_W = 8n + 1. \tag{7}$$

OpenVSP has four inputs for wings and propeller blades to cluster panels toward the leading edge, trailing edge, root, and tip. Values of 1 indicate no clustering (i.e., unit strength panel distribution), values between 0 and 1 increase the density of panels towards the edges while values greater than 1 spread the panels out.

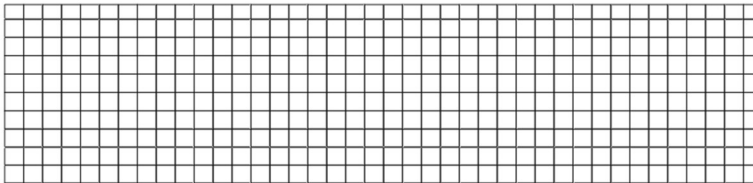
B. Mesh Convergence Study Variables

The mesh convergence studies presented in this section investigate the convergence of results with respect to three variables: the total number of panels, the ratio of the number of spanwise panels to the number of chordwise panels, and the clustering of the panels.

Two ratios of number of spanwise to number of chordwise panels were explored. These ratios were chosen to correspond to individual panel aspect ratios of approximately 1:1 (i.e., square) and 2:1. A 1:1 approximate panel aspect ratio is typically best practice for a VLM, but a 2:1 approximate panel aspect ratio was also explored because it results in fewer panels and, therefore, shorter run times. An example of the wing mesh with the two panel aspect ratios applied with uniform panel distribution (no clustering) is provided in Fig. 5 and a similar example with wing edge clustering is provided in Fig. 6. Visualization of the top of the wing camber surface (leading edge up) for the two approximate panel aspect ratios with clustering applied at the edges. To calculate the Num_U and Num_W values, Num_W inputs were first chosen to meet the constraints of Eq. (6) or (7); second, Num_U inputs were chosen to produce the desired panel aspect ratio. This procedure resulted in a constant ratio of number of spanwise to number of chordwise panels for each panel aspect ratio explored.

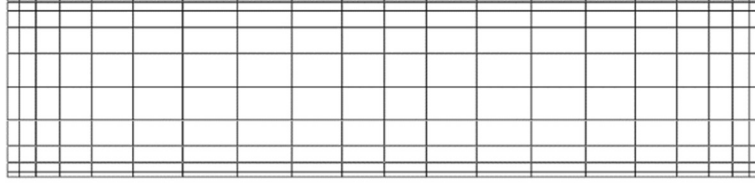


a) Approximate 2:1 panel aspect ratio with no clustering (200 panels).

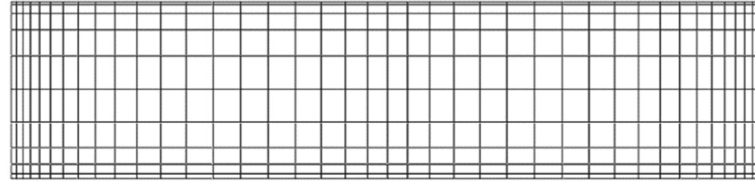


b) Approximate 1:1 panel aspect ratio with no clustering (400 panels).

Fig. 5 Visualization of the top of the wing camber surface (leading edge up) for two panel aspect ratios with uniform panel distribution.



a) Approximate 2:1 panel aspect ratio with the leading edge and trailing edge clustering set to 0.2 and the wing tip clustering set to 0.25 (200 panels).



b) Approximate 1:1 panel aspect ratio with the leading edge and trailing edge clustering set to 0.2 and the wing tip clustering set to 0.25 (400 panels).

Fig. 6 Visualization of the top of the wing camber surface (leading edge up) for the two approximate panel aspect ratios with clustering applied at the edges.

To calculate the total number of panels from Num_U and Num_W , three calculations were performed: first, since Num_U and Num_W correspond to the number of nodes, each input must be reduced by 1 in order to calculate the number of panels along the semispan and along the chord; second, for the wing, the number of panels along the semispan ($Num_U - 1$) is multiplied by two to obtain the total number of spanwise panels because the wing was modeled with X-Z symmetry activated; and third, since the chordwise number of panels accounts for panels on both the upper and lower surfaces of the wing and the VLM uses a thin surface geometry representation, ($Num_W - 1$) was divided by two. The final mesh parameters used in the mesh convergence study are presented in Table 6 for the wing and in Table 7 for the propeller blades.

Table 6 Mesh Parameters Studied for the Wing in Isolation Using the VLM

Approximate Panel Aspect Ratio	Spanwise to Chordwise Panels Ratio	Num_U	Num_W	Number of Spanwise Panels $2(Num_U - 1)$	Number of Chordwise Panels $\frac{Num_W - 1}{2}$	Total Number of Panels
2:1	2:1	7	13	12	6	72
		11	21	20	10	200
		19	37	36	18	648
		31	61	60	30	1800
		47	93	92	46	4232
		57	113	112	56	6272
		63	125	124	62	7688
		67	133	132	66	8712
		71	141	140	70	9800
1:1	4:1	21	21	40	10	400
		37	37	72	18	1296
		61	61	120	30	3600
		77	77	152	38	5776
		93	93	184	46	8464
		125	125	248	62	15376
		133	133	264	66	17424
		141	141	280	70	19600

Table 7 Mesh Parameters Studied for Propeller in Isolation Using the VLM

Approximate Panel Aspect Ratio	Spanwise to Chordwise Panels Ratio	Num_U	Num_W	Number of Spanwise Panels ($Num_U - 1$)	Number of Chordwise Panels $\frac{Num_W - 1}{2}$	Total Number of Panels per Propeller Blade
2:1	2:1	9	9	8	4	32
		17	17	16	8	128
		25	25	24	12	288
		33	33	32	16	512
		41	41	40	20	800
		49	49	76	24	1152
		65	65	64	32	2048
1:1	4:1	17	9	16	4	64
		33	17	32	8	256
		49	25	48	12	576
		65	33	64	16	1024
		97	49	96	24	2304

C. Wing in Isolation

The mesh study for the wing in isolation was performed at angles of attack of 0 and 10 degrees. Two clustering settings were studied for each panel aspect ratio. The first clustering setting was without clustering. The second clustering setting was with chordwise and spanwise clustering applied; the leading edge and trailing edge clustering were set to 0.2, the tip clustering was set to 0.25 and the root clustering was set to 1.0 (there was unit root clustering because the wing is symmetric.)

Predictions for lift, induced drag, and pitching moment at 0 and 10 degrees angle of attack are presented in Fig. 7 and Fig. 8, respectively. There is a spike in the curves at the point that corresponds to a Num_W value of 133 (8712 and 17424 panels for the 2:1 and 4:1, respectively), regardless of the value of Num_U or the clustering setting (this spike is more pronounced in cases with clustering). The reason for the spike is unknown; the spike was also found to occur at a Num_W value of 133 when the airfoil was replaced with a NACA 2215 airfoil as a test. Therefore, when selecting mesh parameters to use for the studies in Section VI, Num_W values close to 133 were avoided.

Apart from the spike, the curves seem to asymptote toward converged values. However, changing the number of spanwise to number of chordwise panels ratio seems to drive the converged value to different magnitudes. The same effect is not seen when changing the clustering setting as it does not seem to affect the magnitude of the converged value. The 4:1 number of spanwise to number of chordwise panels ratio was selected instead of the 2:1 number of spanwise to number of chordwise panels ratio setting because the 4:1 ratio curves appear to reach a higher degree of convergence before the spike occurs. Between the two clustering settings, the 4:1 ratio with clustering curves show less steady convergence in the region before the spike. Thus, the 4:1 ratio with no clustering setting was chosen. Based on these results, the wing mesh settings selected for the studies in Section VI are 8,464 panels, 4:1 number of spanwise panels to number of chordwise panels ratio, and no clustering.

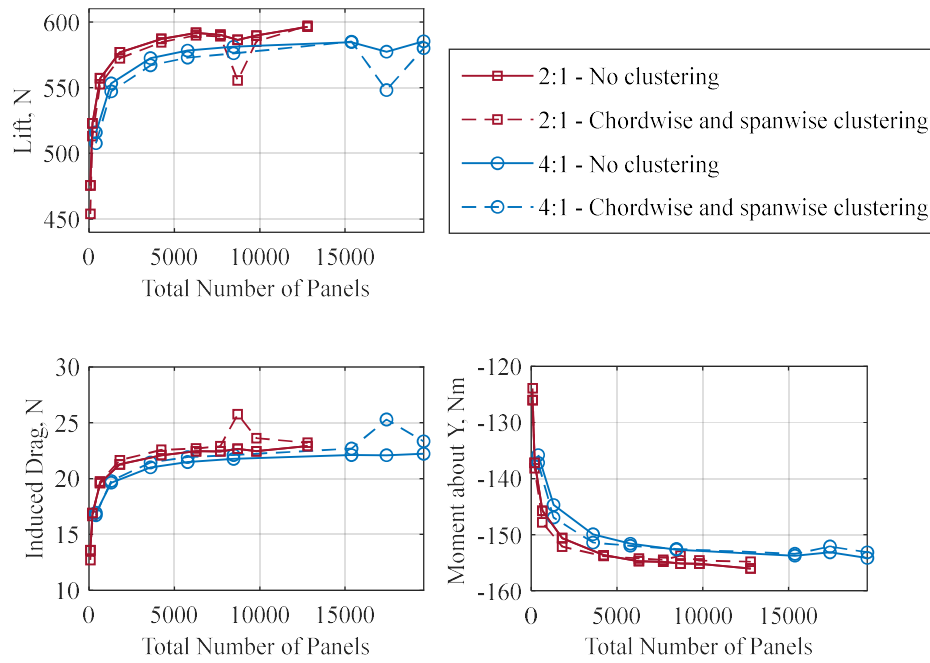


Fig. 7 Results from isolated wing mesh study using the VLM at 0 degrees angle of attack; the ratios presented are the ratios of number of spanwise to number of chordwise panels.

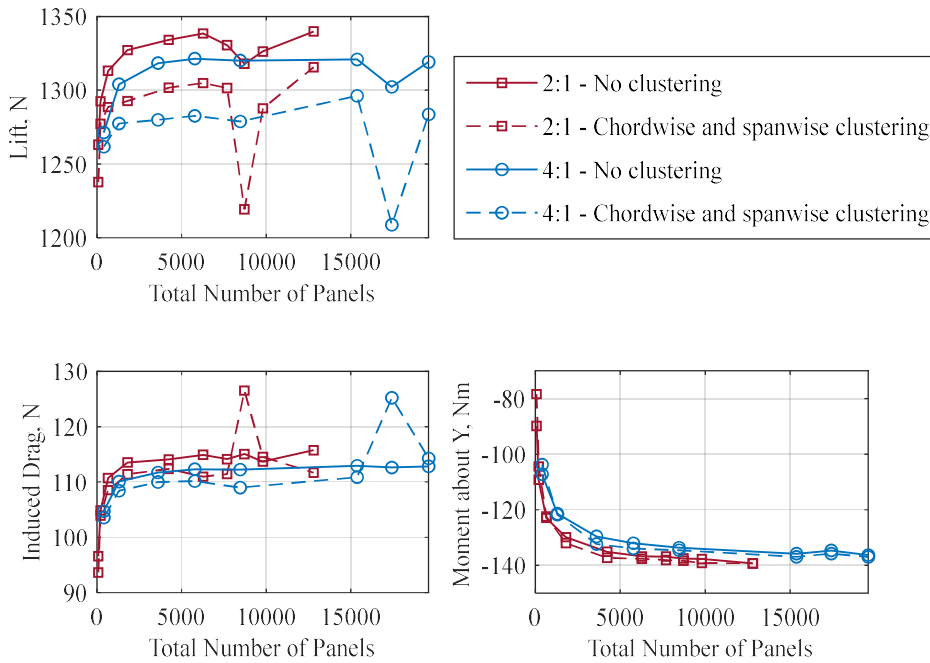


Fig. 8 Results from isolated wing mesh study using the VLM at angle of attack of 10 degrees; the ratios presented are the ratios of number of spanwise to number of chordwise panels.

D. Propeller in Isolation

For the propeller in isolation, unsteady (time-dependent) analyses were run for three propeller revolutions. The isolated propeller mesh study was informed by the isolated wing mesh study. Three settings were tested for the isolated propeller mesh study: the 2:1 number of spanwise panels to number of chordwise panels ratio with clustering in both directions, and the 4:1 number of spanwise panels to number of chordwise panels ratio, first, with no clustering, and, second, with clustering in both directions. The Num_U and Num_W values were chosen in order to satisfy Eq. 7. When clustering was applied, the leading edge clustering and trailing edge clustering were set to 0.25, and the tip clustering and root clustering were set to 0.2.

Predictions for forces and moments at 0 and 10 degrees angle of attack are presented in Fig. 9 and Fig. 10, respectively. Moments are referenced about the center of the propeller. The forces in the Y and Z directions and moments about the Y and Z axes should be approximately zero for 0 degrees angle of attack; the 4:1 number of spanwise to number of chordwise panels ratio with no clustering curves show the best results for these loads. For the forces in the X direction and moments about the X axis, the 4:1 ratio with no clustering curves showed the best asymptotic convergence behavior. Changing the clustering settings seemed to drive the converged value to different magnitudes and using different ratio of spanwise to number of chordwise panels ratios did not seem to affect the magnitude of the converged value. This is the opposite outcome as the one seen for the isolated wing. The propeller mesh settings for the studies in Section VI utilize 576 panels per blade, the 4:1 number of spanwise to number of chordwise panels ratio, and no clustering, as this point corresponds to the lowest number of panels in the converged region.

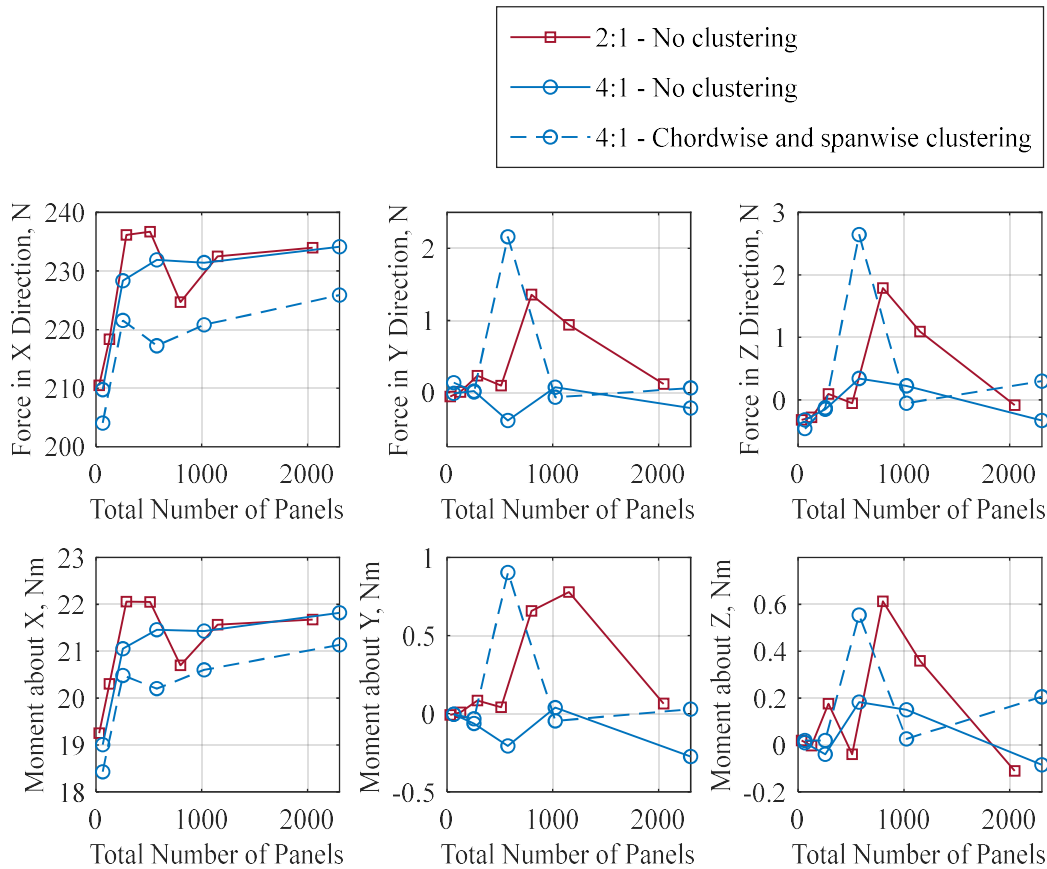


Fig. 9 Results from isolated propeller mesh study using VLM at angle of attack of 0 degrees; the ratios presented are the ratios of number of spanwise to number of chordwise panels.

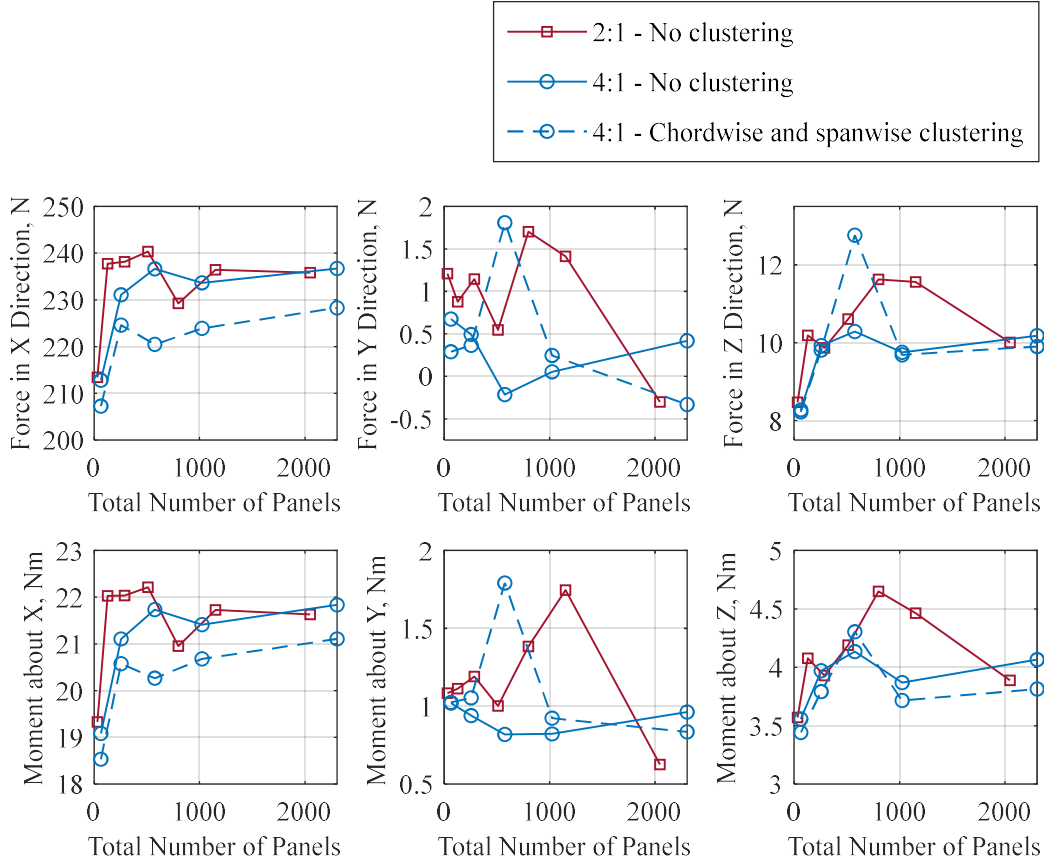


Fig. 10 Results from isolated propeller mesh study using VLM at angle of attack of 10 degrees; the ratios presented are the ratios of number of spanwise to number of chordwise panels.

VI. Results

This section presents VSPAERO force and moment predictions obtained by implementing the geometry meshes recommended in Section V and compares these predictions with those from OVERFLOW and RoBIN. Analyses were performed for the wing in isolation, the propeller in isolation, and Configurations 1 and 2. All VSPAERO runs were performed with VLM, and the propeller was modeled either as an actuator disk or rotating blades in Configurations 1 and 2. The VSPAERO and RoBIN drag predictions represent induced drag, whereas the OVERFLOW drag predictions represent a total drag that accounts for viscous effects.

A. Wing in Isolation

Fig. 11 presents the forces and moments predicted by VSPAERO and OVERFLOW for the isolated wing. OVERFLOW analyses predict that lift is linear with angle of attack up to approximately 10 degrees, after which the slope begins to decrease due to viscous effects. VSPAERO lift predictions are also linear up to 10 degrees angle of attack, and match OVERFLOW predictions reasonably well with a 1.5% overprediction at 10 degrees angle of attack, although the linear slope predicted by VSPAERO is slightly less steep than OVERFLOW, resulting in an overprediction of lift at -5 degrees angle of attack of 55.3%. The lift curve slope begins to taper off at higher angles of attack past 10 degrees, which is common for the inviscid lift curve of a finite span wing.

VSPAERO underpredicts drag relative to OVERFLOW; the offset between the VSPAERO and OVERFLOW predictions increases with angle of attack, as expected when comparing inviscid and viscous drag predictions.

The pitching moment predicted by VSPAERO achieves a similar order of magnitude, but trends in the opposite direction compared to the OVERFLOW predictions. The rolling and yawing moment are expected to be approximately 0 Nm for a symmetric wing; however, they somewhat deviate away from zero at angles of attack greater than 10 degrees, suggesting that the analysis did not reach a perfectly symmetric solution.

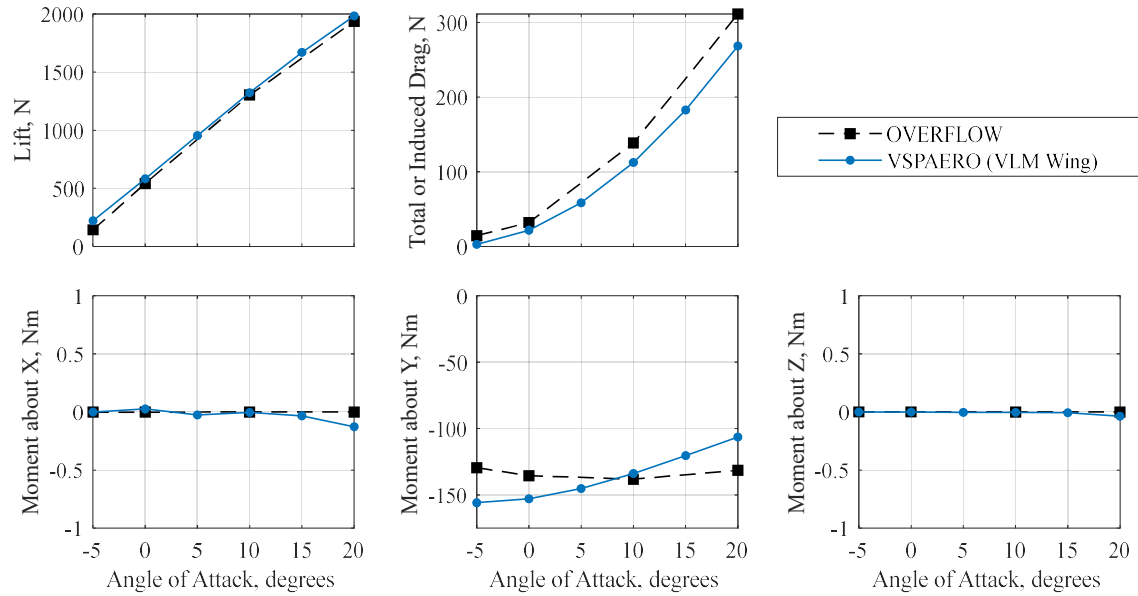


Fig. 11 Isolated wing forces and moments about the wing quarter chord.

B. Propeller in Isolation

The forces and moments predicted by VSPAERO, RoBIN, and OVERFLOW for the isolated propeller using VLM are presented in Fig. 12. Lift and drag are presented as well as forces resolved in the X, Y, and Z directions for ease of comparison with the later propeller-blown wing plots. The moments are presented about the center of the propeller. VSPAERO thrust predictions (equivalent to negative force in the X direction) trend well relative to OVERFLOW, but with an approximately constant 10% overprediction in thrust. RoBIN also overpredicts thrust relative to OVERFLOW; the discrepancy between the VSPAERO and RoBIN predictions may be a result of the differences in the implementation of VLM or the differences in mesh and time step settings.

The VSPAERO predictions for torque trend well with OVERFLOW, with an approximately constant overprediction of 2%. VSPAERO does not capture side forces well: both OVERFLOW and RoBIN show side forces becoming increasingly negative with angle of attack, whereas VSPAERO predictions remain at approximately 0 N for all angles of attack. VSPAERO predictions for the normal force match OVERFLOW well; pitching and rolling moment predictions follow a similar trend to OVERFLOW, but with sleeper slopes.

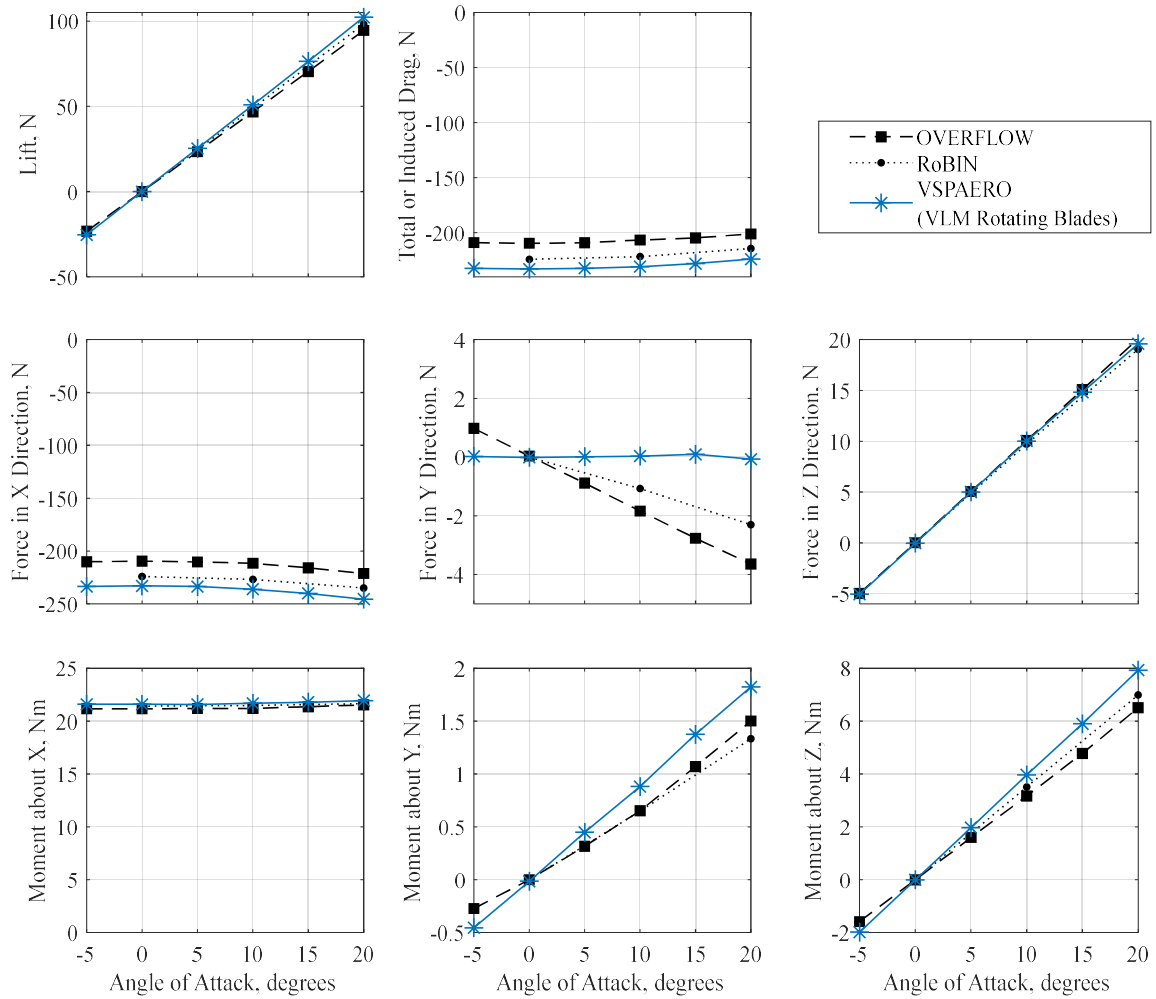


Fig. 12 Isolated propeller forces and moments about the propeller center.

C. Propeller-blown Wing

The total forces and moments predicted for Configurations 1 and 2 are presented in Fig. 13 and Fig. 14, respectively, with moments presented about the wing quarter chord. Next, the breakdown of these total forces and moments into wing and propeller components for each configuration are presented in Fig. 15 through Fig. 18: the wing component forces and moments about the wing quarter chord are presented in Fig. 15 and Fig. 16; the propeller component forces and moments about the propeller center are presented in Fig. 17 and Fig. 18.

Total Forces and Moments

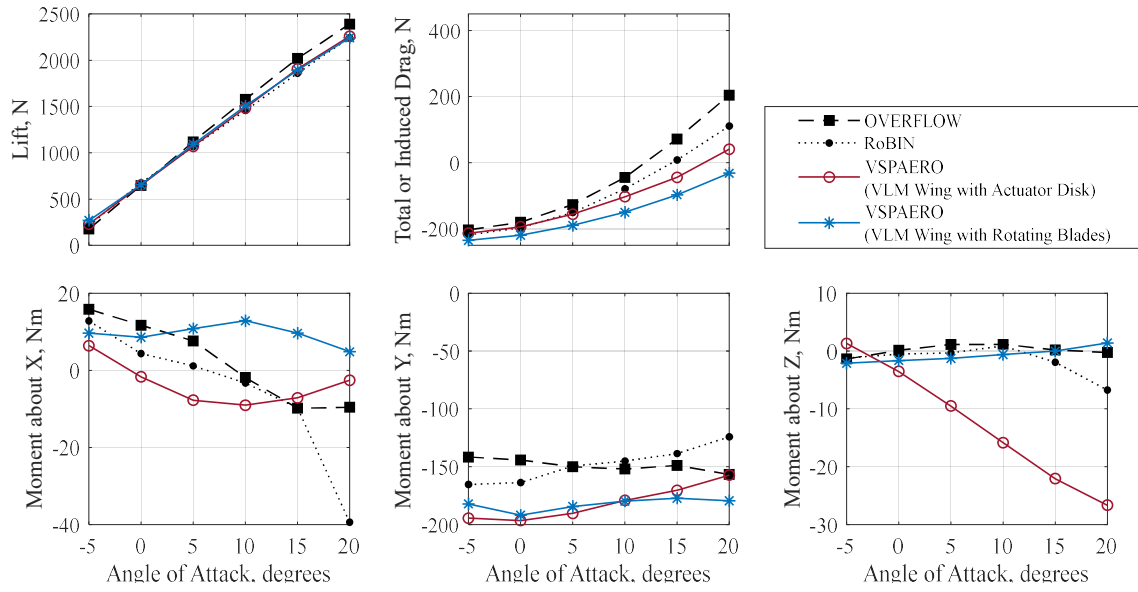


Fig. 13 Configuration 1 (midspan propeller): total forces and moments.

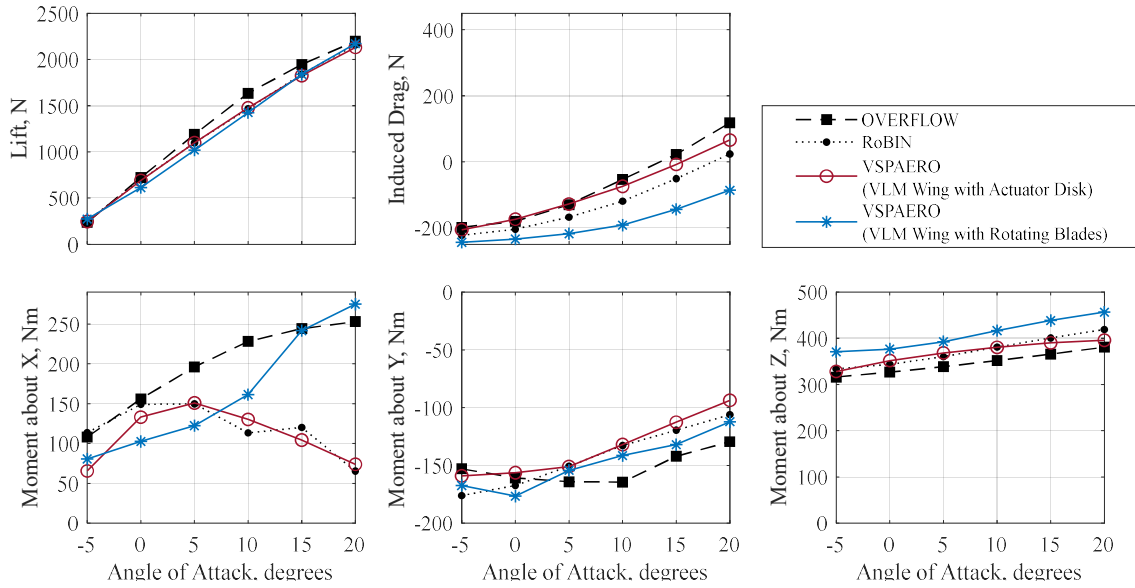


Fig. 14 Configuration 2 (wingtip propeller): total forces and moments.

Wing Component Forces and Moments

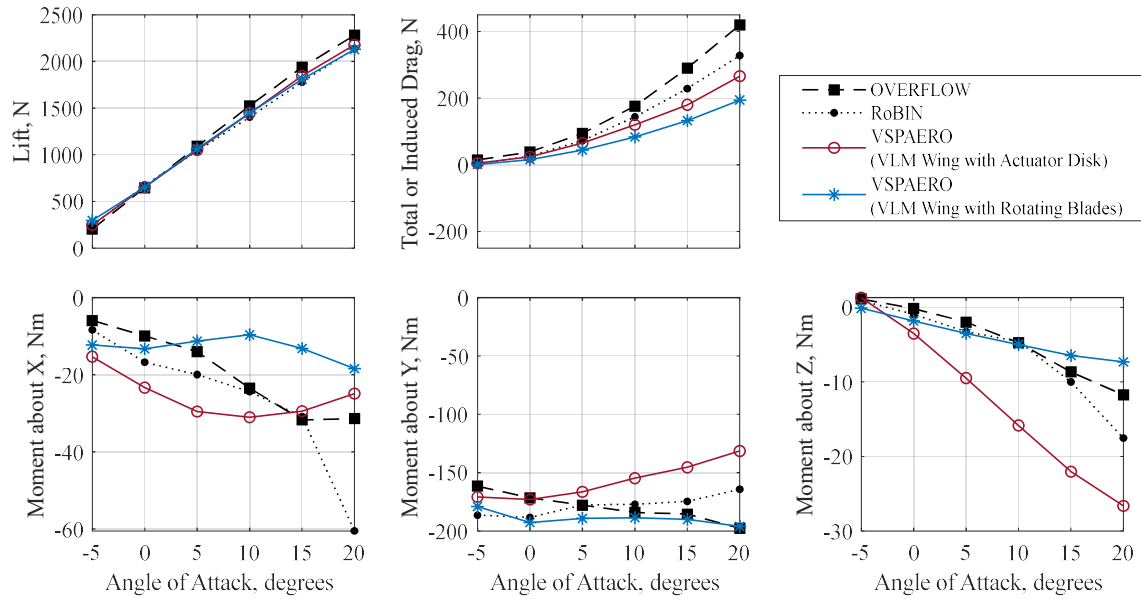


Fig. 15 Configuration 1 (midspan propeller): wing component forces and moments about the wing quarter chord.

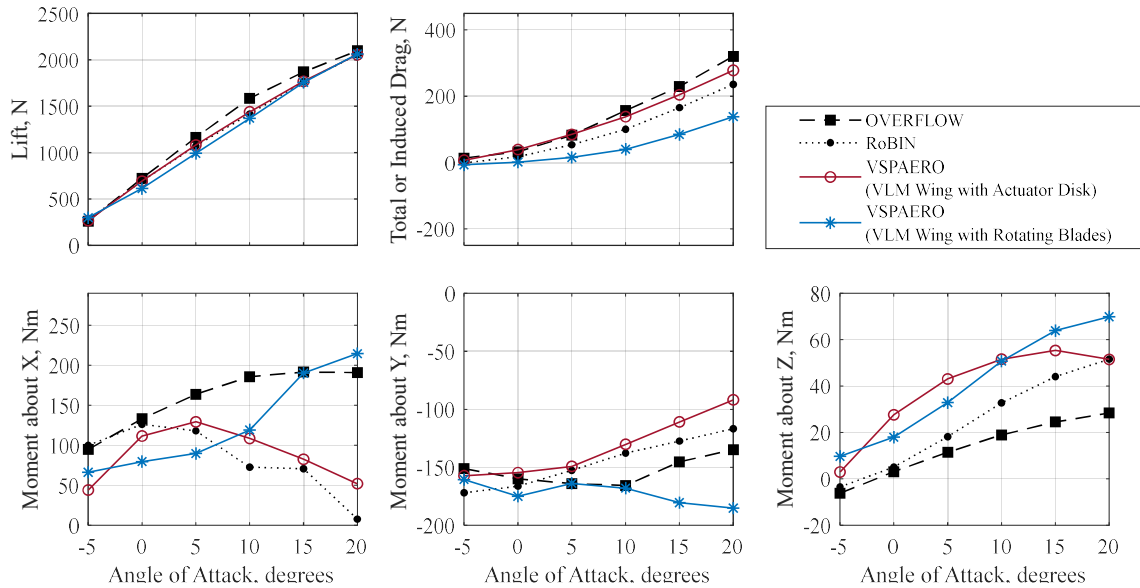


Fig. 16 Configuration 2 (wingtip propeller): wing component forces and moments about the wing quarter chord.

Propeller Component Forces and Moments

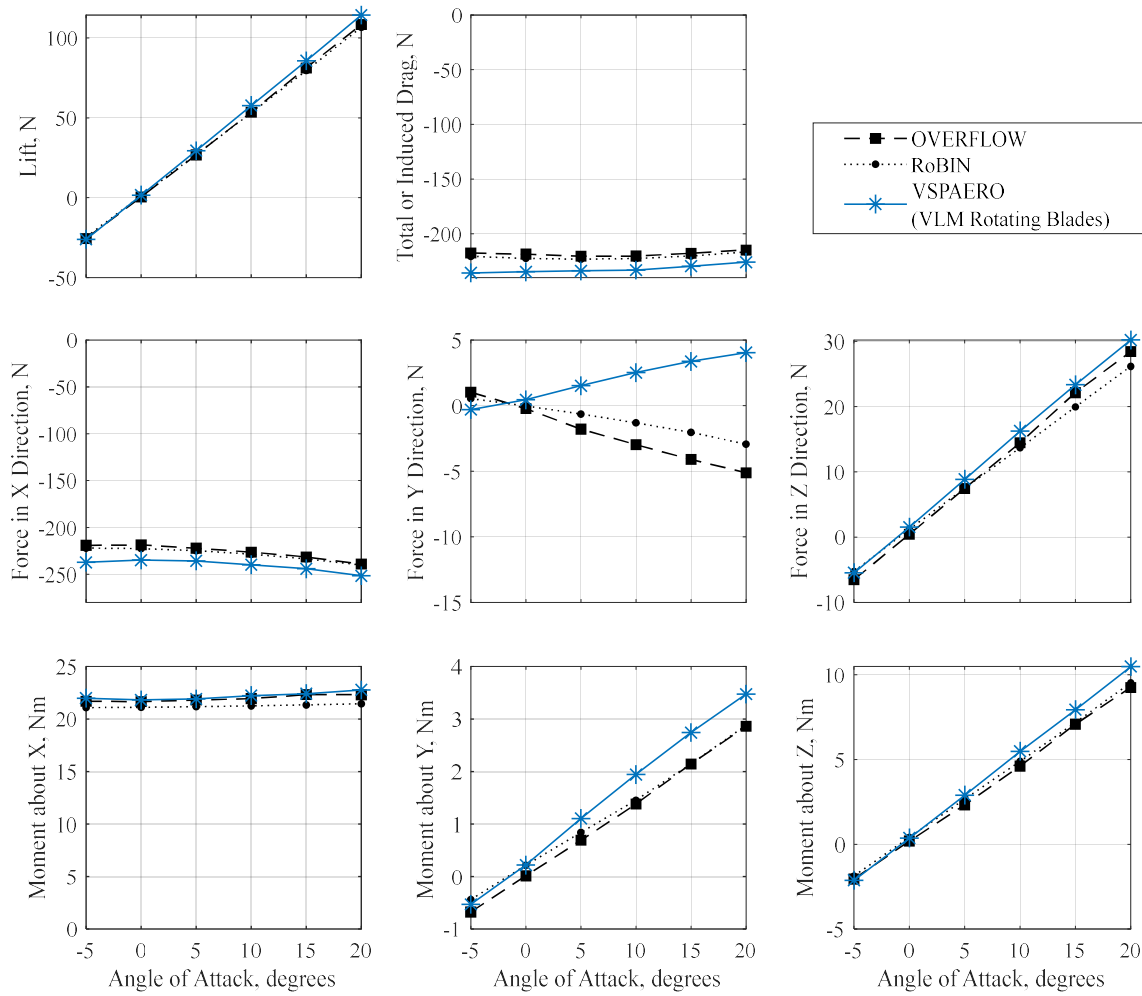


Fig. 17 Configuration 1 (midspan propeller): propeller component forces and moments about the center of the propeller.

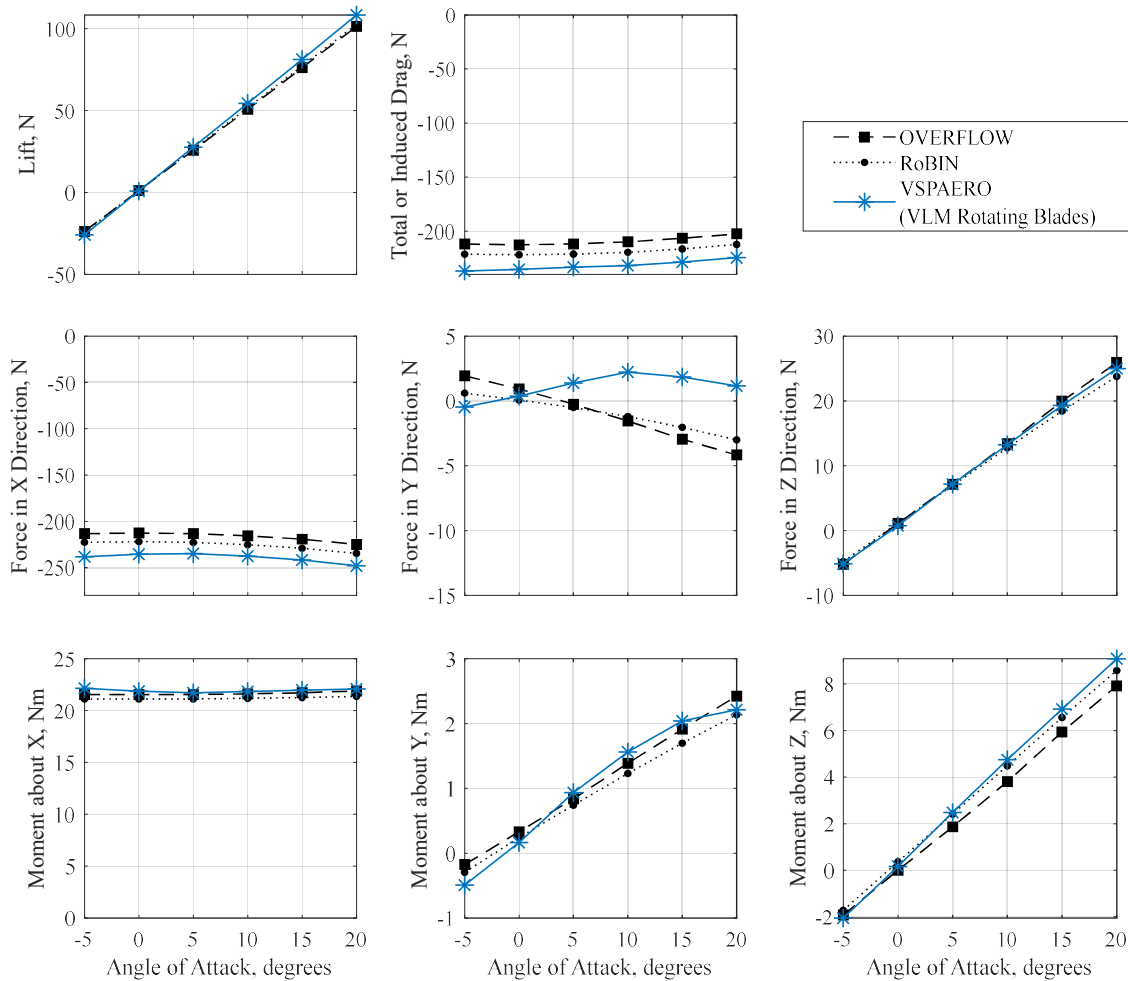


Fig. 18 Configuration 2 (wingtip propeller): propeller component forces and moments about the center of the propeller.

OVERFLOW predictions show that the total and wing component lift slopes are linear up to 10 degrees angle of attack for both configurations, and then the slope decreases with increasing angle of attack. The lift curve slope for Configuration 2 falls off more than for Configuration 1, indicating that the location of the midspan propeller encourages more of the flow to remain attached over the wing, thus delaying separation.

For Configuration 1, the VSPAERO lift predictions for runs with rotating blades and runs with an actuator disk were similar to each other. VSPAERO total and wing component lift predictions follow the OVERFLOW lift predictions closely up to 15 degrees angle of attack, with an overprediction in total lift of 1.1% at 0 degrees and an underprediction of 5.8% at 10 degrees angle of attack. For Configuration 2 with the propeller modeled as rotating blades, the total and wing component lift slopes show underpredictions relative to OVERFLOW even at low angles of attack, resulting in an underprediction in total lift of 15% at 0 degrees angle of attack and 13% underprediction at 10 degrees angle of attack. For Configuration 2 with the propeller modeled as an actuator disk, VSPAERO total lift predictions show underpredictions relative to OVERFLOW of 4.3% at 0 degrees angle of attack and 9.6% at 10 degrees angle of attack.

Generally, VSPAERO underpredicts drag relative to OVERFLOW, and the discrepancy between VSPAERO and OVERFLOW predictions increases with angle of attack, as expected due to viscous effects that increase with angle of attack. Induced drag predictions from VSPAERO runs with an actuator disk follow OVERFLOW predictions more closely than runs with rotating blades, which may be attributed to the fact that propeller thrust and torque components derived from OVERFLOW were manually added back into the actuator disk forces and moments predictions.

VSPAERO runs with rotating blades underpredict the total drag across all angles of attack compared to the other VLM methods. This underprediction of total drag largely stems from the contribution of the underprediction of drag for the wing component (which makes up 95% and 90% of the total difference at 20 degrees angle of attack, for Configurations 1 and 2, respectively) and, to a lesser extent, the overprediction of propeller component thrust (which makes up for 5% and 10% of the total difference at 20 degrees angle of attack for Configurations 1 and 2, respectively). The VSPAERO yawing moment prediction for Configuration 2 also appears to be overpredicted. As explained in Ref. [5], this is likely due to the overprediction of thrust on the advancing side of the propeller.

The VSPAERO total and wing component moment predictions perform inconsistently relative to OVERFLOW, suggesting that moments are generally difficult to predict with VLM. The VSPAERO moments predictions vary depending on whether runs are with rotating blades or an actuator disk. This stems from how propeller-wing interactions are captured differently for runs with rotating blades than with an actuator disk. VSPAERO runs with rotating blades capture the effects of the propeller blade passing through the air in revolutions, while actuator disks give steady assumptions of the slipstream flow. At higher angles of attack, the assumptions employed in the actuator disk model begin to break down, thereby degrading the accuracy of the actuator disk wake model, which explains the divergence in moments predictions for VSPAERO runs with an actuator disk.

The total pitching moment predicted by OVERFLOW appears reasonably constant across the range of angles of attack for both Configurations 1 and 2. For Configuration 2, the VSPAERO total pitching moment predictions for runs with an actuator disk and with rotating blades are very similar in trend and magnitude. For Configuration 1, the total pitching moments predicted by VSPAERO show greater disparity between the two methods, likely because the influence of the midspan propeller wake on the wing is greater than that of the wingtip propeller. For both configurations, the pitching moment predicted by VSPAERO does not trend with the OVERFLOW predictions.

The differences between the total and wing component moments predicted by VSPAERO runs with rotating blades as opposed to VSPAERO runs with an actuator disk are seen especially in the rolling and yawing moments for both configurations. The yawing moment predictions for Configuration 2 show that VSPAERO runs with an actuator disk predict an unexpected fall off in magnitude at 20 degrees angle of attack, while runs with rotating blades continue to trend with OVERFLOW. The wing component rolling moments predicted by both VSPAERO methods do not trend consistently with the OVERFLOW predictions. There is also inconsistency between the wing component rolling moment predictions by RoBIN and by VSPAERO runs with rotating blades.

VII. Computation Time

The RoBIN, OVERFLOW, and VSPAERO predictions presented were generated using different computing resources. Thus, only an informal account of the computational times is provided. The OVERFLOW cases were run in parallel on the NASA Langley Research Center K3-subcluster using 10 Intel Xeon Processor E5-2670 CPUs (total of 160 threads), and completed in approximately 60 hours [5].

The RoBIN cases were run in sequence on a server with two Intel Xeon Platinum 8160 CPUs, but the Biot-Savart calculations were accelerated via four NVIDIA Tesla P4 GPUs. The isolated propeller analyses (400 panels per blade and 72 time-steps per revolution) required approximately 20 minutes per case. The resolution settings that were selected for the propeller-blown wing cases (1,600 panels for the wing) required approximately 30 minutes per case. [5].

The VSPAERO cases were run on a server with four Intel Xeon Gold 6148 CPUs. Each VSPAERO run used 16 logical cores, and several runs were performed at the same time.

The isolated wing VLM mesh convergence studies had runtimes from 1 minute to 40 minutes per case (72 to 19,600 panels). The mesh settings selected for the subsequent isolated wing analyses (8,464 panels) required approximately 5 minutes per angle of attack.

Runtimes for the VSPAERO mesh convergence studies for the isolated propeller modeled as rotating blades in the VLM ranged from 2 minutes to 185 minutes per case (32 to 2304 panels per blade and 24 time-steps per revolution, 3 revolutions). The mesh settings selected for subsequent isolated propeller analyses required approximately 160 minutes per angle of attack (576 panels per blade and 24 time-steps per revolution, 8 revolutions).

For the final results, the runtimes for VSPAERO VLM wing with the propeller modeled as an actuator disk averaged 4 to 8 minutes per case, whereas the VSPAERO VLM wing with rotating blades cases had an average runtime of approximately 370 minutes per angle of attack.

VIII. Conclusions

This study evaluated an open-source, vortex-lattice method (VLM) flow solver, VSPAERO, in its ability to model two different propeller-blown wing configurations with either an actuator disk or propeller. Predictions were compared against another VLM solver, RoBIN, and a high-fidelity CFD solver, OVERFLOW. A mesh sensitivity study was conducted prior to running simulations to determine appropriate wing and propeller blade mesh parameters. Analyses were first performed for the wing in isolation and propeller in isolation, and then for Configuration 1 (a rectangular wing with midspan propeller) and Configuration 2 (a rectangular wing with wingtip propeller).

Four important conclusions were determined in conducting the mesh studies. First, it was found that for the wing in isolation, a spike occurred in the mesh study results when the number of mesh nodes in the chordwise direction, Num_W, was equal to 133. Second, it was found that a large number of panels (8,464 panels on the wing and 576 panels per blade) were required to achieve converged results. Third, applying different mesh settings caused predictions to converge to different values. Fourth, it was found that the 1:1 approximate panel aspect ratio with no clustering seemed to achieve the best convergence for both geometries.

The VSPAERO lift predictions for the isolated wing matched OVERFLOW predictions reasonably well in the inviscid region with a 7.6% overprediction at 0 degrees angle of attack reducing to a 1.5% overprediction at 10 degrees angle of attack. VSPAERO predictions for the isolated propeller showed an approximately constant 10% overprediction in thrust and 2% overprediction in torque. For Configuration 1, the VSPAERO lift predictions for runs with the propeller modeled as rotating blades and as an actuator disk were similar to each other in trend and magnitude with an overprediction in total lift of up to 5.8% at 10 degrees angle of attack. For Configuration 2, VSPAERO runs with rotating blades underpredict the total lift by 13% at 10 degrees angle of attack relative to OVERFLOW and runs with an actuator disk show underpredictions of 9.6% at 10 degrees angle of attack. VSPAERO moments predictions tend to be inconsistent relative to OVERFLOW, which makes VSPAERO less useful for determining precise dynamics or trim behaviors, although the predicted moments are generally within the expected range of values by 15-20%. VSPAERO runs with an actuator disk required 98% less runtime than VSPAERO runs with rotating blades.

For the propeller-blown wing configurations studied, the agreement between VSPAERO and OVERFLOW predictions (particularly for force predictions at small angles of attack) indicates that VSPAERO can be valuable in the conceptual and early design phases where capturing the approximate solution quickly is of higher importance than obtaining a highly accurate solution. Further studies are recommended to investigate the wider applicability of VSPAERO in modeling a variety of other propeller-wing interactions and/or flight conditions.

Acknowledgments

This work was supported by the NASA Langley Research Center Innovation Fund for Internal Research and Development, and by the NASA Internships, Fellowships & Scholarships (NIFS) Program. The authors would like to acknowledge Brandon Litherland for his assistance with VSPAERO and for providing OVERFLOW datasets, Xiaofan Fei for his assistance with VSPAERO and for providing RoBIN datasets, and Beau Pollard for providing OVERFLOW datasets. VSPAERO inputs were also guided by the OpenVSP Google Group [18] and the OpenVSP 2020 Workshop [7].

References

- [1] National Aeronautics and Space Administration, "Advanced Air Mobility," Aeronautics Research Mission Directorate, 28 Apr 2021. [Online]. Available: <https://www.nasa.gov/aam>. [Accessed 18 May 2021].
- [2] VSPAERO, "Software Package, Version 3.22.0," NASA, <http://openvsp.org/>, 2021.
- [3] Fei, X., Litherland, B., German, B., "Development of an Unsteady Vortex Lattice Method to Model Propellers at Incidence," *AIAA Journal (Pending Review)*, 2020.
- [4] OVERFLOW, OVERset grid FLOW solver, "Software Package, Version 2.3," NASA, URL: <https://overflow.larc.nasa.gov/>.
- [5] Fei, X., "The Causes of Propeller Pitching Moment and the Conditions for Its Significance," Georgia Institute of Technology, 2021.
- [6] "OpenVSP, Vehicle Sketch Pad.", Software Package, Version 3.22.0, NASA,, "URL: <https://openvsp.org>".
- [7] "OpenVSP Workshop 2020.", "<http://openvsp.org/wiki/doku.php?id=pastworkshops>," 2020.
- [8] Farokhi, S., "Aircraft Propulsion, 2nd Edition," Wiley, 2014.

- [9] Conway, J., "Analytical solutions for the actuator disk with variable radial distribution of load," *Journal of Fluid Mechanics*, pp. 297, 327-355, 1995.
- [10] Whiteside, S. K. S., Pollard, B. P., Antcliff, K. R., Zawodny, N. S., Fei, X., Silva, C. and Medina, G. L., "Design of a Tiltwing Concept Vehicle for Urban Air Mobility," NASA Technical Memorandum, Hampton, VA, 2021.
- [11] Katz, J. and Plotkin, A., *Low-Speed Aerodynamics*, 2nd Edition, Cambridge University Press, 2001.
- [12] Nichols, R. and Buning, P., "User's Manual for OVERFLOW 2.2, v.2.2m," 2017. URL: <https://overflow.larc.nasa.gov/home/users-manual-for-overflow-2-2/>.
- [13] CGT, Chimera Grid Tools, "Software Package, Version 2.2," NASA, URL: <https://software.nasa.gov/software/ARC-16025-1B>.
- [14] Henrick, A.K., Aslam T.D., and Powers, J. M., "Mapped weighted essentially non-oscillatory schemes: Achieving optimal order near critical points," *Journal of Computational Physics*, vol. 207, no. 2, pp. 542-567, 2005.
- [15] Viken, J. K., Viken S., Deere, K. A., and Carter, M., "Design of the Cruise and Flap Airfoil for the X-57 Maxwell Distributed Electric Propulsion Aircraft," *AIAA Paper 2017-3922*, June 2017.
- [16] Patterson M. D., Borer N. K., and German, B., "A Simple Method for High-Lift Propeller Conceptual Design," in *AIAA Paper 2016-0770*, January 2016.
- [17] "OpenVSP Hangar.", Vehicle Model Database [online database], "URL: <http://hangar.openvsp.org/vspfiles/526>".
- [18] "OpenVSP Google Group.", Community Forum [online forum], "URL: <https://groups.google.com/forum/#!forum/openvsp>".